Colorado State University, NIH, and the donors of the Petroleum Research Fund, administered by the American Chemical Society, for partial support of this research (to D.C.C.). We thank John Vaughan for helpful discussions with the kinetic analysis and Branka Ladanyi for reading this manuscript. We thank the Colorado State University Regional NMR Center funded by NSF Grant CHE-8616437 for access to the 500-MHz NMR spectrometer.

Conformational Dynamics of Proline Residues in Antamanide. *J* Coupling Analysis of Strongly Coupled Spin Systems Based on E.COSY Spectra

Z. L. Mádi, C. Griesinger, and R. R. Ernst*

Contribution from the Laboratorium für Physikalische Chemie, Eidgenössische Technische Hochschule, 8092 Zürich, Switzerland. *Received July 11, 1989*

Abstract: The conformational dynamics and individual conformations of the four proline residues in the cyclic decapeptide antamanide in solution are determined from vicinal proton coupling constants combined with the measurement of carbon-13 relaxation times. The coupling constants, obtained by a least-squares analysis of a two-dimensional E.COSY spectrum, are interpreted in terms of generalized Karplus equations. It is found that Pro^3 and Pro^8 are conformationally rigid, while Pro^2 and Pro^7 are mobile with a significant population of a second conformation. The time constants that govern the conformational dynamics of the proline residues are estimated to be between 30 and 40 ps.

1. Introduction

It is known that the conformational dynamics of peptides can be relevant for their biological activity. Often, binding to a substrate leads to additional conformational constraints. In many cases, it is the interconversion rate between conformations that determines the rate of complex formation.

The cyclic decapeptide antamanide, cyclo-(-Val^1-Pro^2-Pro^3-Ala^4-Phe^5-Phe^6-Pro^7-Pro^8-Phe^9-Phe^{10}-), is known to exhibit several conformations which can dynamically interconvert.[1] This molecule has been studied in great detail by various research groups. The crystal structure has been determined by Karle et al.[2] The structure in solution was investigated by Tonelli,[3] Dorman and Bovey,[4] Pook et al.,[5] and most recently in an extensive study by Müller[6] and Kessler et al.[7-10] It was discovered in 1973 by Patel[11] that antamanide is involved in a dynamic equilibrium between different backbone conformations. The rate constant of interconversion ($\sim 10^6$ s^{-1}) has later been measured by Burgermeister et al.[12,13] by means of ultrasonic absorption experiments. It has also been found that complexation with ions, such as Na^+ and Ca^{2+}, inhibits the conformational dynamics.[12] Evidently this type of motion is related to its binding properties.

In addition, antamanide shows degrees of motion that are associated with the rotational isomerism of side chains, such as phenylalanine ring flips. Rate processes that can be associated with this type of motion have been observed in ultrasonic absorption measurements.[13] These processes have correlation times on the order of the inverse nuclear Larmor frequency in typical NMR experiments and are therefore relaxation-active.

This paper is concerned with a further type of conformational dynamics in antamanide, the proline ring flips. This process is expected, if it occurs at all, to be considerably faster than the backbone motion and the side-chain mobility mentioned above. The conformation of proline rings has already been determined in different types of peptides.[14-22] It has been found that the free proline ring without external constraints can occur in two almost equal-energetic conformations that rapidly interconvert.[18,19] Upon introduction of external constraints, such as in cyclic peptides or in proteins with a confined structure, the conformational mobility can be restricted or inhibited. Conditions for rigidity versus flexibility have been summarized by Cung et al.[22]

In antamanide it has been found that two of the four proline rings, Pro^3 and Pro^8, are fixed in the $^{\beta}_{\gamma}$T conformation,[7,8] while the other two proline systems, Pro^2 and Pro^7, could not be analyzed due to strong coupling in the proton resonance spectrum which complicates the spectrum to an extent that inhibits a straightforward analysis.

In this paper, we present a complete analysis of the structure and dynamics of all four proline ring systems in antamanide. A new strategy is introduced that combines the knowledge of proton spin coupling constants and carbon-13 relaxation times. A recently developed least-squares computer-fitting procedure[23] is used to

(1) Wieland, T. H.; Lüben, G.; Ottenheym, H.; Faesel, J.; de Vries, J. X.: Konz, W.; Prox, A.; Schmid, J. *Angew. Chem.* **1968**, *80*, 209.
(2) Karle, I. L.; Karle, I.; Wieland, T.; Burgermeister, W.; Faulstich, H.; Witkop, B. *Proc. Natl. acad. Sci. U.S.A.* **1973**, *70*, 1836.
(3) Tonelli, A. E. *Biochemistry* **1973**, *12*, 689.
(4) Dorman, D. E.; Bovey, F. A. *J. Org. Chem.* **1973**, *38*, 2379.
(5) Pook, K.-H.; Birr, C.; Wieland, T. *Int. J. Pept. Protein Res.* **1980**, *15*, 32.
(6) Müller, A. Dissertation NMR spektroskopische Untersuchung der Konformation von Antamanid in apolaren Lösungsmitteln, Universität Frankfurt, 1984.
(7) Kessler, H.; Müller, A.; Oschkinat, H. *Magn. Reson. Chem.* **1985**, *23*, 844.
(8) Kessler, H.; Griesinger, C.; Müller, A.; Lautz, J.; van Gunsteren, W. F.; Berendsen, H. J. G. *J. Am. Chem. Soc.* **1988**, *110*, 3399.
(9) Kessler, H.; Müller, A.; Pook, K.-H. *Liebigs Ann.* **1989**, 903.
(10) Kessler, H.; Bats, J. W.; Lautz, J.; Müller, A. *Liebigs Ann.* **1989**, 913.
(11) Patel, D. J. *Biochemistry* **1973**, *12*, 667.
(12) Burgermeister, W.; Wieland, T.; Winkler, R. *Eur. J. Biochem.* **1974**, *44*, 305.
(13) Burgermeister, W.; Wieland, T.; Winkler, R. *Eur. J. Biochem.* **1974**, *44*, 311.
(14) Abraham, R. J.; McLauchlan, K. A. *Mol. Phys.* **1962**, *5*, 195, 513.
(15) Deber, C. M.; Torchia, D. A.; Blout, E. R. *J. Am. Chem. Soc.* **1971**, *93*, 4893.
(16) Deslauriers, R.; Smith, I. C. P.; Walter, R. *J. Biol. Chem.* **1974**, *249*, 7006.
(17) DeTar, D. F.; Luthra, N. P. *J. Am. Chem. Soc.* **1977**, *99*, 1232.
(18) London, R. E. *J. Am. Chem. Soc.* **1978**, *100*, 2678.
(19) Shekar, S. C.; Easwaran, K. R. K. *Biopolymers* **1982**, *21*, 1479.
(20) Sarkar, S. K.; Torchia, D. A.; Kopple, K. D.; VanderHart, D. L. *J. Am. Chem. Soc.* **1984**, *106*, 3328.
(21) Sarkar, S. K.; Young, P. E.; Torchia, D. A. *J. Am. Chem. Soc.* **1986**, *108*, 6459.
(22) Cung, M. T.; Vitoux, B.; Marraud, M. *New J. Chem.* **1987**, *11*, 503.
(23) Mádi, Z. L.; Ernst, R. R. *J. Magn. Reson.* **1988**, *79*, 513.

0002-7863/90/1512-2908$02.50/0

Table I. Coupling Constants (Hz) in the Four Proline Residues of Antamanide Determined by Least-Squares Fitting of an E.COSY Spectrum[a]

	Pro^2	Pro^3	Pro^7	Pro^8
$J(\alpha\beta_1)$	7.97 ± 0.05	1.12 ± 0.05	8.81 ± 0.03	0.88 ± 0.03
$J(\alpha\beta_2)$	7.40 ± 0.05	8.49 ± 0.02	5.78 ± 0.03	8.08 ± 0.01
$J(\alpha\gamma_1)$	−0.63 ± 0.05	0.29 ± 0.02	−0.88 ± 0.04	0.62 ± 0.02
$J(\alpha\gamma_2)$	−0.21 ± 0.06	−1.08 ± 0.04	−0.08 ± 0.03	−0.56 ± 0.02
$J(\alpha\delta_1)$	1.20 ± 0.08	−0.67 ± 0.11	−0.32 ± 0.05	*b*
$J(\alpha\delta_2)$	−0.54 ± 0.09	−0.48 ± 0.12	−0.71 ± 0.05	*b*
$J(\beta_1\beta_2)$	−12.56 ± 0.07	−12.87 ± 0.04	−12.87 ± 0.03	−12.48 ± 0.05
$J(\beta_1\gamma_1)$	4.80 ± 0.06	2.36 ± 0.02	5.93 ± 0.02	1.38 ± 0.10
$J(\beta_1\gamma_2)$	7.08 ± 0.07	6.47 ± 0.03	7.39 ± 0.03	6.42 ± 0.07
$J(\beta_1\delta_1)$	0.81 ± 0.11	0.73 ± 0.04	0.14 ± 0.03	−0.56 ± 0.06
$J(\beta_1\delta_2)$	−0.19 ± 0.07	−0.57 ± 0.05	−0.42 ± 0.03	0.36 ± 0.07
$J(\beta_2\gamma_1)$	7.08 ± 0.05	6.76 ± 0.02	7.04 ± 0.02	6.83 ± 0.01
$J(\beta_2\gamma_2)$	8.96 ± 0.06	12.00 ± 0.03	7.52 ± 0.02	12.97 ± 0.04
$J(\beta_2\delta_1)$	−0.09 ± 0.12	−0.57 ± 0.05	−0.55 ± 0.03	−0.02 ± 0.06
$J(\beta_2\delta_2)$	0.00 ± 0.07	0.05 ± 0.04	0.12 ± 0.03	−0.41 ± 0.02
$J(\gamma_1\gamma_2)$	−12.34 ± 0.07	−12.85 ± 0.03	−12.31 ± 0.02	−13.10 ± 0.06
$J(\gamma_1\delta_1)$	4.60 ± 0.11	2.11 ± 0.07	5.35 ± 0.02	7.34 ± 0.06
$J(\gamma_1\delta_2)$	7.02 ± 0.05	7.61 ± 0.07	6.99 ± 0.02	1.46 ± 0.09
$J(\gamma_2\delta_1)$	7.61 ± 0.09	8.53 ± 0.04	7.34 ± 0.02	10.88 ± 0.09
$J(\gamma_2\delta_2)$	8.50 ± 0.06	10.29 ± 0.04	7.36 ± 0.02	8.81 ± 0.09
$J(\delta_1\delta_2)$	−10.00 ± 0.07	−12.29 ± 0.11	−9.91 ± 0.03	−11.91 ± 0.04

[a] The rms errors are indicated. [b] The couplings $J(\alpha\delta)$ cannot be determined from the E.COSY spectrum by inspection[26] because of the absence of visible α,δ cross peaks.

analyze the strongly coupled proton seven-spin systems of the proline rings and to determine the full set of coupling constants. The analysis is based on a two-dimensional E.COSY spectrum[24-26] that contains sufficient information, yet has a much simpler structure than a conventional two-dimensional COSY spectrum.[27]

On the basis of modified Karplus relations for vicinal coupling constants that take into account the electronegativity of the substituents attached to the considered HCCH fragment in the proline ring,[28-30] the observed average coupling constants are interpreted in terms of a dynamic equilibrium between two proline ring conformations with unequal population. In combination with carbon-13 relaxation time measurements, it is finally possible to determine the rate constants of the conformational dynamics.

2. Determination of Proline Spin Coupling Constants

The proton coupling constants of the four residues have been determined based on a 300 MHz E.COSY (exclusive correlation spectroscopy) spectrum, recorded by standard procedures.[24-26] It is known that E.COSY cross peaks exhibit a particularly simple multiplet structure that is ideally suited for a detailed analysis in terms of J coupling constants.[24-26] An excerpt relevant for the present analysis is shown in Figure 1a. It contains the $\gamma\delta$ cross peaks of Pro^2, Pro^3, and Pro^7 and the $\alpha\beta$ cross peaks of Pro^2, Pro^7, and Pro^8. It is apparent that cross peaks of Pro^2, Pro^3, and Pro^7 overlap, while the Pro^8 cross peaks are well separated. The analysis of the proline spin systems is performed in the order Pro^8, Pro^3, Pro^2, and Pro^7 by means of a least-squares fitting program described in ref 23.

Proline-8. The spin system of Pro^8 is weakly coupled and can be analyzed by inspection of the various cross peaks. The manually determined coupling constants are contained in Table I.[26] The vicinal couplings are in agreement with the coupling constants[7] found initially by the DISCO (Differences and Sums within COSY spectra) method.[31,32]

Table II. The Eight Possible Assignments (A1–A8) for the β, γ, and δ Protons in Proline (See Figure 2)

stereochemical position	assignment							
	A1	A2	A3	A4	A5	A6	A7	A8
H_α	α	α	α	α	α	α	α	α
H_β^c	β_1	β_1	β_1	β_1	β_2	β_2	β_2	β_2
H_β^t	β_2	β_2	β_2	β_2	β_1	β_1	β_1	β_1
H_γ^c	γ_1	γ_1	γ_2	γ_2	γ_1	γ_1	γ_2	γ_2
H_γ^t	γ_2	γ_2	γ_1	γ_1	γ_2	γ_2	γ_1	γ_1
H_δ^c	δ_1	δ_2	δ_1	δ_2	δ_1	δ_2	δ_1	δ_2
H_δ^t	δ_2	δ_1	δ_2	δ_1	δ_2	δ_1	δ_2	δ_1

Proline-3. In the Pro^3 spin system, the two δ protons are strongly coupled. Therefore only the coupling constants $J_{\alpha\beta_1}$, $J_{\alpha\beta_2}$, $J_{\alpha\gamma_1}$, $J_{\alpha\gamma_2}$, $J_{\beta_1\beta_2}$, $J_{\beta_1\gamma_1}$, $J_{\beta_2\gamma_1}$, $J_{\beta_1\gamma_2}$, and $J_{\beta_2\gamma_2}$ could be extracted by inspection from the E.COSY spectrum.[26] The remaining coupling constants have been determined iteratively by least-squares fitting of those parts of the four $\gamma\delta$ cross peaks in Figure 1a that do not overlap with cross peaks of the other proline residues.[23] On the basis of the coupling constants, contained in Table I, it was then possible to compute the entire $\gamma\delta$ cross peak multiplets shown in Figure 1b and to subtract the Pro^3 contribution from the original spectrum in Figure 1a to obtain the spectrum of Figure 1c that reveals the contributions of Pro^2, Pro^7, and Pro^8 only.

Proline-2. Strong coupling among the protons β_1 and γ_1 as well as β_2 and γ_2 and overlap of cross peaks required the determination of all coupling constants by fitting the $\alpha\beta$, $\gamma\delta$, and $\delta_1\delta_2$ cross peaks in the edited spectrum of Figure 1c, avoiding the regions in which overlap with cross peaks of Pro^7 was obvious. The starting values for the fitting were $^2J_{HH} = -12$, $^3J_{HH} = 6.9$, and $^4J_{HH} = 0$ Hz. The simulated Pro^2 cross peaks based upon the determined coupling constants are shown in Figure 1d. By subtracting this spectrum from the spectrum shown in Figure 1c, the edited spectrum of Figure 1e is obtained that contains exclusively contributions from Pro^7 and Pro^8.

Proline-7. On the basis of the edited spectrum of Figure 1e, the $\gamma\delta$ cross peaks were fitted together with $\alpha\beta$ cross peaks. The initial parameter values for the fit were chosen in the same way as for Pro^2. The computed Pro^7 $\gamma\delta$ cross peaks, based on the values in Table I, are shown in Figure 1f.

For convergence of the fits, 23, 21, and 20 iteration steps were necessary for the determination of the coupling constants of Pro^3, Pro^2, and Pro^7, respectively.

3. Assignment of Resonances and Coupling Constants

For the three pairs of diastereotopic protons, labeled β_1, β_2, γ_1, γ_2, and δ_1, δ_2 in Table I, there are eight possible assignments to the stereochemical cis and trans positions β^c, β^t, γ^c, γ^t, and δ^c, δ^t in Figure 2 (cis and trans refer to the position of the H_α on the proline ring). The different assignments are labeled A1–A8 and are defined in Table II.

The coupling constants for the residues Pro^3 and Pro^8 allow a clear distinction between gauche and trans arrangement of the protons. Starting with the $\alpha\beta$ couplings, it is possible to assign β_1 in both residues to the position β^t with a dihedral angle close to 90° based on the small coupling constants $J_{\alpha\beta_1} = 1.12$ Hz for Pro^3 and $J_{\alpha\beta_1} = 0.88$ Hz for Pro^8. H_{γ_2} is in trans position to H_{β_2} ($J_{\beta_2\gamma_2} = 12.00$ Hz for Pro^3, $J_{\beta_2\gamma_2} = 12.97$ Hz for Pro^8), and H_{δ_1} is in trans position to H_{γ_2} ($J_{\gamma_2\delta_1} = 10.29$ Hz for Pro^3, $J_{\gamma_2\delta_1} = 10.88$ for Pro^8). This completes the assignment for these two residues and leads to assignment A7 in Table II in agreement with the assignments given in refs 6 and 10.

The assignment of the observed resonances for Pro^2 and Pro^7 is not as straightforward. The only information available from previous work indicates a cis arrangement within the pairs Pro^2H_α and H_{β_1}, Pro^7H_α and H_{β_1}, and $Pro^7H_{\gamma_1}$ and H_{δ_1}, based on NOE measurements.[6,10] Further NOE's could not be determined in these residues due to cross peak overlap. This suggests as possible

(24) Griesinger, C.; Sørensen, O. W.; Ernst, R. R. *J. Am. Chem. Soc.* **1985**, *107*, 6394.
(25) Griesinger, C.; Sørensen, O. W.; Ernst, R. R. *J. Chem. Phys.* **1986**, *85*, 6837.
(26) Griesinger, C.; Sørensen, O. W.; Ernst, R. R. *J. Magn. Reson.* **1987**, *75*, 474.
(27) Ernst, R. R.; Bodenhausen, G.; Wokaun, A. Principles of NMR in One and Two Dimensions; Clarendon Press: Oxford, 1987.
(28) Haasnoot, C. A. G.; de Leeuw, F. A. A. M.; Altona, C. *Tetrahedron* **1980**, *36*, 2783.
(29) Haasnoot, C. A. G.; De Leeuw, F. A. A. M.; de Leeuw, H. P. M.; Altona, C. *Org. Magn. Reson.* **1981**, *15*, 43.
(30) Haasnoot, C. A. G.; de Leeuw, F. A. A. M.; de Leeuw, H. P. M.; Altona, C. *Biopolymers* **1981**, *20*, 1211.
(31) Freeman, R.; Oschkinat, H. *J. Magn. Reson.* **1984**, *60*, 164.
(32) Oschkinat, H.; Kessler, H. *Angew. Chem.* **1985**, *95*, 689; *Angew. Chem. Int. Ed. Engl.* **1985**, *21*, 690.

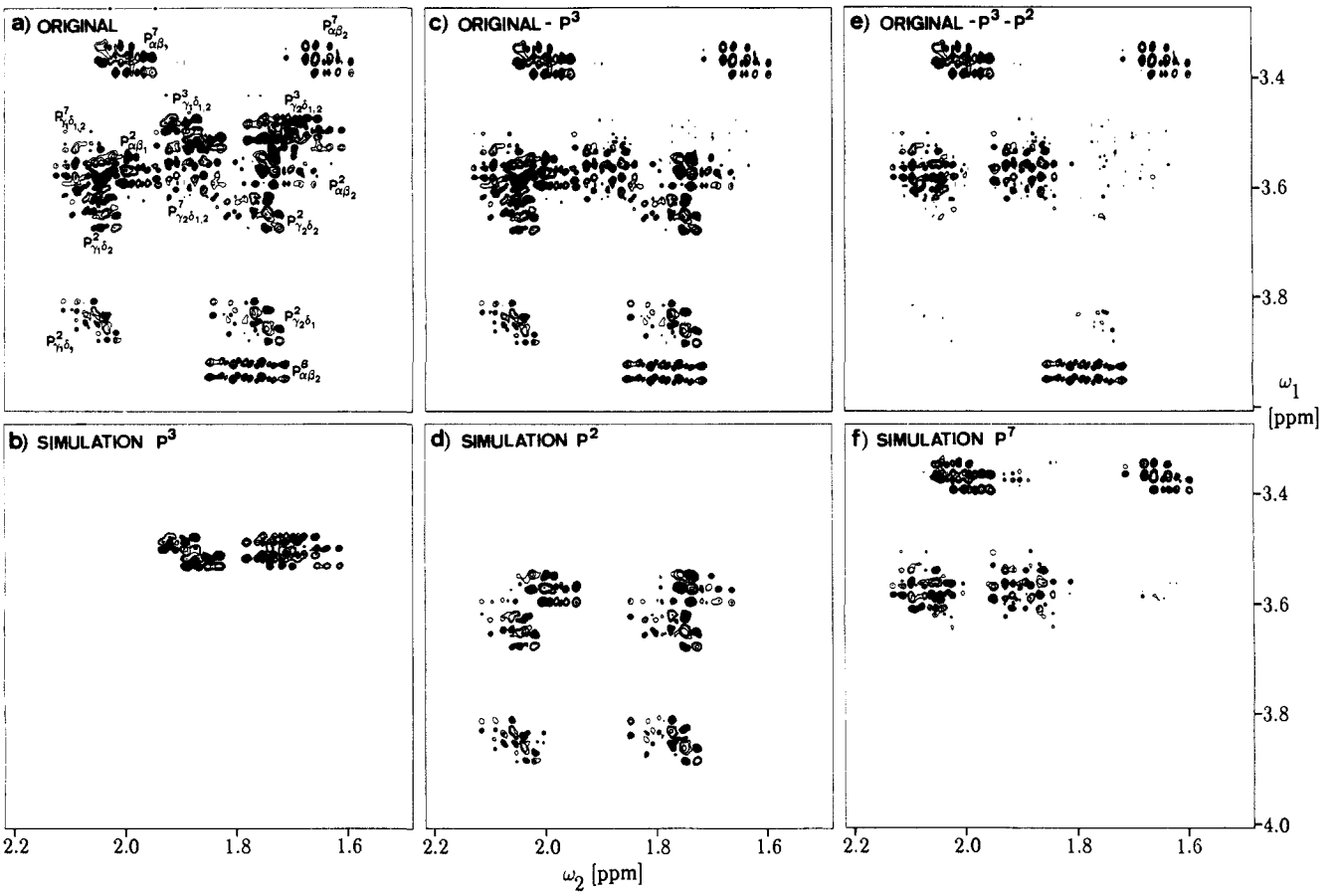

Figure 1. Excerpt of the 300-MHz E.COSY proton resonance spectrum of a 20 mM solution of antamanide in chloroform recorded on a home-built NMR spectrometer. The spectral region contains $H_\alpha H_\beta$ and $H_\gamma H_\delta$ cross peaks of Pro^2, Pro^3, Pro^7, and Pro^8. Negative peaks are shown in black. (b) Pro^3 contribution to the E.COSY spectrum of (a) calculated from the data in Table I that have been obtained by an iterative computer fit of parts of the spectrum in (a). (c) The experimental E.COSY spectrum of antamanide of (a) minus the computed contribution of Pro^3 shown in (b). (d) Pro^2 contribution to the residual E.COSY spectrum of (c) calculated from the data in Table I that have been obtained by an iterative computer fit of parts of the spectrum in (c). (e) Experimental E.COSY spectrum of antamanide of (a) minus the contributions of Pro^2 and Pro^3 shown in (b) and (d). (f) Pro^7 contribution to the residual E.COSY spectrum of (e) calculated from the data in Table I that have been obtained by an iterative computer fit of parts of the spectrum in (e).

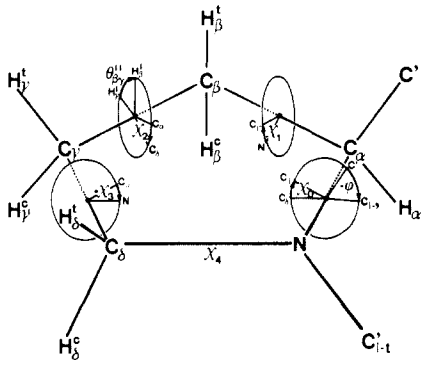

Figure 2. Notation used in this paper for the designation of nuclei and angles in L-proline.

assignments A1, A2, A3, or A4 for Pro^2 and A1 or A4 for Pro^7. The most likely assignments for all four proline residues will be determined in the following section in connection with the investigation of the conformational dynamics based on an rms deviation criterion that takes into account simultaneously all measured coupling constants.

4. Conformational Equilibrium of Proline Residues

The vicinal coupling constants in Pro^3 and Pro^8 characteristic for gauche and trans arrangements suggest conformational stability. All coupling constants lie in the expected ranges for a rigid conformation. On the other hand, the limited spread of the vicinal coupling constants in Pro^2 and Pro^7 and the consequent difficulties of stereospecific assignment suggest conformational dynamics. This possibility shall be investigated in this section based on a comparison with theoretically predicted coupling constants that are dynamically averaged. We limit the conformational freedom to the possible existence of two discrete conformations with possibly unequal populations in a rapidly exchanging dynamic equilibrium. This is clearly a model assumption as the data are insufficient to rule out a multiconformational equilibrium.

Table III. Parameters (a_1–a_7) for the Modified Karplus Equation (Eq 1) Following Ref 30

	two substituents	three substituents
a_1	13.89 Hz	13.22 Hz
a_2	−0.98 Hz	−0.99 Hz
a_3	0	0
a_4	1.02 Hz	0.87 Hz
a_5	−3.40 Hz	−2.46 Hz
a_6	14.9	19.9
a_7	0.24	0

The conformational analysis relies on modified Karplus equations which relate vicinal coupling constants $^3J_{HH}$ and interproton dihedral angles θ in proline residues as described in refs 28–30:

$$^3J_{HH} = a_1 \cos^2\theta + a_2 \cos\theta + a_3 + \sum_i \Delta x_i' \{a_4 + a_5 \cos^2(\xi_i\theta + a_6|\Delta x_i'|)\} \quad (1)$$

The parameters a_1–a_6 are given in Table III for HCCH fragments with two and three additional substituents that are different from H. The summation in eq 1 runs over all these substituents with

Table IV. Relation between the Dihedral Angle of Vicinal Proton Pairs and the Respective Torsion Angle χ and the Parameters ξ_i That Define the Sign of the Substituent Contributions in Eq 1[30]

		$\alpha\beta^c$	$\alpha\beta^t$		$\beta^c\gamma^t$	$\beta^t\gamma^t$	$\beta^c\gamma^c$	$\beta^t\gamma^c$		$\gamma^t\delta^c$	$\gamma^t\delta^t$	$\gamma^c\delta^c$	$\gamma^c\delta^t$
θ_{HH}		$\chi_1 - 1.7°$	$\chi_1 - 122.9°$		$\chi_2 - 121.7°$	$\chi_2 - 0.6°$	$\chi_2 + 0.5°$	$\chi_2 - 121.6°$		$\chi_3 + 122.2°$	$\chi_3 + 0.7°$	$\chi_3 + 0.1°$	$\chi_3 - 121.5°$
ξ_i	C′:	−1	+1	C_α:	+1	−1	+1	−1	C_β:	−1	−1	+1	+1
	N:	+1	+1	C_δ:	+1	+1	−1	−1	N:	−1	+1	−1	+1
	C_γ:	+1	+1										

Table V

P	−72°	−54°	−36°	−18°	0°	18°	36°	54°	72°
conformation	${}^{\alpha}_{N}T$	${}^{\alpha}E$	${}^{\alpha}_{\beta}T$	${}_{\beta}E$	${}^{\gamma}_{\beta}T$	${}^{\gamma}E$	${}^{\gamma}_{\delta}T$	${}_{\delta}E$	${}^{N}_{\delta}T$
P	108	126	144	162	180	198	216	234	252
conformation	${}^{N}_{\alpha}T$	${}_{\alpha}E$	${}^{\beta}_{\alpha}T$	${}^{\beta}E$	${}^{\beta}_{\gamma}T$	${}_{\gamma}E$	${}^{\delta}_{\gamma}T$	${}^{\delta}E$	${}^{\delta}_{N}T$

their effective electronegativity differences $\Delta x_i'$ that are given by the expression

$$\Delta x_i' = \Delta x_i - a_7 \sum_k \Delta x_k \qquad (2)$$

where Δx_i is the electronegativity difference of the substituent with respect to hydrogen $\Delta x_H = 0$, $\Delta x_C = 0.40$, and $\Delta x_N = 0.85$.[33] The second term in eq 2 takes into account the influence of the electronegativity Δx_k of all substituents k that are attached to substituent i (secondary substituent effect). The parameter ξ_i in eq 1 that determines the relative orientation of the substituent i with respect to the HCCH fragment is specified in Table IV together with the relations between the proton–proton dihedral angles θ_{HH} and the torsional angles χ_1, χ_2, and χ_3.

The conformational mobility in five-membered rings is limited and can be described by two parameters, the pseudorotation phase P and the pseudorotation radius χ_{max}.[28-30] The pseudorotation phase P determines the angular position along the ring with maximum out-of-plane puckering amplitude χ_{max}. The reference line $P = 0$ intersects the C_β–C_γ bond. On the basis of these two parameters, it is possible to express the five endocyclic torsion angles χ_j

$$\chi_j = \chi_{max} \cos\,(P + 4\pi(j-2)/5) \qquad j = 0, 1, 2, 3, 4 \quad (3)$$

Since the ring is odd-numbered, the pseudorotation has effectively a period of 4π as expressed by the angle $2P$ (with the definition range $0 \le P < 2\pi$). When the direction $2P$, for example, intersects the C_α–C_β bond, we have a twist conformation ${}^{\beta}_{\alpha}T$ or ${}^{\alpha}_{\beta}T$, while an envelope conformation ${}_{\alpha}E$ or ${}^{\alpha}E$ results when the direction $2P$ passes through C_α. This leads to the identification of conformations and pseudorotation phases P in Table V.

In order to decide upon the most likely one of the eight possible assignments in Table II and to determine the population of the two dynamically interchanging ring conformations, a grid search has been performed for each of the four proline residues for each of the eight possible assignments. The pseudorotation angles P_1 and P_2 of the two conformations have been varied in steps of 4° between 4° and 360°, while the two pseudorotation radii $\chi_{max}^{(1)}$ and $\chi_{max}^{(2)}$ have been varied between 2° and 70° in steps of 2°. The population p_1 of conformation 1 was varied between 0 and 100% in steps of 5%. For each conformational pair, the vicinal coupling constants were computed based on eq 1, averaged according to the populations p_1 and p_2, and compared with the experimental values. The rms deviation σ_J determines the quality of the fit.

Table VI presents the sets of parameters that lead to the minimum rms deviation σ_J for the four proline residues for each of the eight possible assignments. In addition to the dynamic average between two conformations, also the computed values assuming a single rigid conformation have been included.

For Pro[3] and Pro[8], we find that assignment A7 leads to the best fit, in accordance with the preliminary discussion in section 3. It is also apparent that allowing for a second conformation does not significantly reduce the rms error in the J coupling constants nor does this conformation obtain a significant population (0.1 for Pro[3] and 0.05 for Pro[8]); for Pro[8] also an unreasonably high value for $\chi_{max}^{(2)}$ (90°) would result. This leads to the conclusion that indeed Pro[3] and Pro[8] seem to have one rigid conformation. The values P and χ_{max} indicate for both residues a ${}^{\beta}_{\gamma}T$ conformation that is shown in Figure 3. The minor conformation for Pro[3] would have ${}_{\gamma}E$ form.

For Pro[2] and Pro[7], on the other hand, the introduction of a second conformation leads to a drastic reduction of the rms error in the coupling constants as is shown by the data in Table VI. In both cases, assignment A1 has the highest probability (Pro[2], $\sigma_J = 0.44$; Pro[7], $\sigma_J = 0.41$), followed by assignment A8 with a slightly increased rms error (Pro[2], $\sigma_J = 0.66$; Pro[7], $\sigma_J = 0.49$). For assignment A8, however, a conformation with an unreasonably high value of χ_{max} (70°) would be involved. In addition, the NOE measurements mentioned in section 3 contradict assignment A8. This further supports the assignment A1. It is remarkable that in both residues, the minor conformation has a significant population (Pro[2], 35%; Pro[7], 45%). The major conformation of Pro[2] is close to ${}^{\gamma}E$ ($P_1 = 13°$), while the minor conformation is in between ${}^{\beta}_{\gamma}T$ and ${}_{\gamma}E$ ($P_2 = 189°$). For Pro[7], the major conformation is again close to ${}^{\gamma}E$ ($P_2 = 25°$), while the minor conformation is close to ${}^{\beta}_{\gamma}T$ ($P_1 = 185°$). The conformations of Pro[2] and Pro[7] are given in Figure 3. The finding of two conformations for Pro[2] and Pro[7] agrees with molecular force field calculations that predict two energy minima close to the conformation found in the present work.[34]

The static conformations of Pro[3] and Pro[8] found in the present work are in reasonable agreement with X-ray data[35] as shown by the endocyclic torsion angles of Table VII. The X-ray structures for Pro[2] and Pro[7] are found to lie between the two dynamically interconverting structures found by NMR. On the basis of a comparison of the torsion angles in Table VII, one may conclude that the X-ray structure of Pro[2] contains 76% contribution of the NMR conformation 1 and 24% of the NMR conformation 2, while in solution the respective populations are 65% and 35%. For Pro[7] one finds in the solid a 71% contribution of the NMR conformation 1 and a 29% contribution of the NMR conformation 2, whereas in solution the populations are 55% and 45%. In solid, there is thus a tendency to favor the minimum energy solution conformation. To confirm this preliminary comparison of NMR and X-ray data and to determine whether a conformational equilibrium is involved in solid state, a careful study of the temperature factors of the X-ray would be necessary. These data[35] are unfortunately unavailable at this time.[36]

There remains the question to be answered whether the conformational dynamics of Pro[2] and Pro[7] in solution is the dynamics of independent proline rings or whether the ring flip is induced by a conformational change of the antamanide backbone. This shall be investigated by an analysis of the carbon-13 T_1 relaxation times.

5. Conformational Dynamics of Proline Rings

The ^{13}C relaxation times of the four proline rings have been measured at 400 MHz proton frequency by a standard inversion-recovery technique with observation in the presence of proton decoupling. The measured relaxation times are collected in Table VIII.

We assume a motional model for spin–lattice relaxation in which the molecule undergoes an isotropic overall rotation with correlation time τ_c. In addition, the proline rings shall exchange with correlation time τ_e between the two presumed conformations.

(33) Huggins, M. L. *J. Am. Chem. Soc.* **1953**, *75*, 4123.

(34) Brüschweiler, R.; Fischer, S.; Roux, B.; Karplus, M. Private communication.

(35) Karle, I. L.; Wieland, T.; Schermer, D.; Ottenheym, H. C. J. *Proc. Natl. Acad. Sci. U.S.A.* **1979**, *76*, 1532.

(36) Karle, I. L. Private communication.

Table VI. Computer-Optimized Structures of the Four Proline Residues for Each of the Eight Possible Peak Assignments A_1–A_8[a]

	one conformation			two conformations					
	χ_{max}	P	σ_J	$\chi^{(1)}_{max}$	P_1	$\chi^{(2)}_{max}$	P_2	p_1	σ_J
				Pro 2					
A1	32	17	2.29	**46**	**13**	**32**	**189**	**0.65**	**0.44**
A2	32	17	3.02	70	25	14	233	0.5	1.11
A3	30	265	3.71	44	353	52	221	0.5	1.42
A4	36	259	3.15	58	217	46	317	0.5	1.13
A5	28	11	3.14	68	5	16	165	0.5	1.15
A6	25	1	3.64	22	221	70	9	0.55	1.44
A7	53	245	3.30	70	357	34	225	0.4	1.221
A8	41	243	2.71	44	233	70	333	0.65	0.664
				Pro 7					
A1	28	33	2.83	**46**	**25**	**34**	**185**	**0.55**	**0.41**
A2	27	38	3.26	26	193	62	33	0.5	0.69
A3	30	236	3.59	28	189	66	29	0.55	0.82
A4	23	236	3.22	54	201	32	353	0.5	0.68
A5	32	342	3.18	70	349	26	233	0.5	0.62
A6	32	334	3.57	70	349	40	241	0.5	0.81
A7	51	26	3.46	48	245	70	345	0.55	0.79
A8	42	269	3.09	70	337	46	245	0.4	0.49
				Pro 3					
A1	73	311	3.36	60	1	60	281	0.6	2.58
A2	54	334	1.66	60	93	60	323	0.2	1.08
A3	90	287	3.33	60	173	60	293	0.4	2.42
A4	90	286	4.45	60	245	60	337	0.5	3.36
A5	56	88	4.42	60	65	50	177	0.5	2.19
A6	51	91	3.28	58	125	60	57	0.5	2.51
A7	**40**	**177**	**0.69**	42	177	46	49	0.9	0.61
A8	43	192	3.04	58	101	60	205	0.4	2.11
				Pro 8					
A1	60	324	3.50	60	9	60	289	0.6	2.90
A2	53	337	1.71	60	85	60	333	0.2	1.26
A3	90	287	3.63	60	173	60	293	0.4	2.87
A4	90	286	4.75	60	333	60	245	0.5	3.84
A5	61	89	4.70	60	181	56	73	0.4	3.47
A6	56	93	3.57	60	57	60	121	0.5	2.96
A7	**42**	**177**	**0.57**	40	177	90	213	0.95	0.53
A8	44	190	3.08	60	109	60	209	0.4	2.35

[a] The pseudorotation radii χ_{max} and pseudorotation phases P (see eq 3) are given for one conformation and for two conformations in dynamic equilibrium with populations p_1 and $p_2 = 1 - p_1$. The rms error σ_J expresses the quality of the agreement with the measured J coupling constants based on eq 1.

Table VII. Comparison of the Proline Ring Conformations Based on NMR and X-ray Data[a]

	Pro[2]			Pro[7]			Pro[3]			Pro[8]	
	X-ray	NMR		X-ray	NMR		X-ray	NMR		X-ray	NMR
p_l		0.65	0.35		0.55	0.45		0.9	0.1		
$\chi_0 \simeq \varphi + 60°$	−1	+4	−5	−9.6	−5.6	−7.6	−9.4	−15	−24	−16	−14
χ_1	−15	−30	+23	11	−22.3	25.7	25	35.2	−4.0	29	33.6
χ_2	26	45	−31.6	−11	41.7	−33.8	−33	−42	+30	−31	−40
χ_3	−26.5	−42	28.5	+6	−45.2	29.2	+27	33	−45	+23	+31
χ_4	+15	23.6	−15	+3	31.4	−13.3	−10	−11	42	−4.5	−10

[a] The endocyclic torsion angles χ_i are given in deg.

The two motional processes are tentatively treated as independent. A possible correlation of the two has to be taken into account only when the two correlation times turn out to be similar.

Expressions for T_1 under these conditions have been given by London[18] and Shekar and Easwaran.[19] By using a slightly modified notation, one finds

$$T_1^{-1} = [1 - 3p_1p_2 \sin^2 \Delta\theta]T_1^{-1}(\tau_c) + 3p_1p_2 \sin^2 \Delta\theta\, T_1^{-1}(\tau_{tot}) \quad (4)$$

with

$$T_1^{-1}(\tau) = \frac{\gamma_H^2\gamma_C^2\hbar^2N}{10r_{CH}^6}\left(\frac{\mu}{4\pi}\right)^2\left\{\frac{3}{2}J(\omega_0^C, \tau) + J(\omega_0^C - \omega_0^H, \tau) + 3J(\omega_0^C + \omega_0^H, \tau)\right\}$$

and $J(\omega,\tau) = 2\tau(1 + \omega^2\tau^2)^{-1}$.

Table VIII. NT_1 ^{13}C Relaxation Times (in ms) of the Carbons in the Four Proline Residues and of the α-Carbons in the Other Residues in Antamanide at 280 K Measured with an Inversion Recovery Sequence (N = number of attached protons)[a]

	Pro[2]	Pro[7]	Pro[3]	Pro[8]
C_α	247 ± 2	242 ± 3	260 ± 3	250 ± 3
C_β	410 ± 10	412 ± 2	311 ± 1	286 ± 4
C_γ	535 ± 2	614 ± 4	336 ± 1	286 ± 1
C_δ	332 ± 4	345 ± 1	292 ± 5	272 ± 5

	Val[1]	Ala[4]	Phe[5]	Phe[6]	Phe[9]	Phe[10]
C_α	249 ± 5	253 ± 2	246 ± 6	243 ± 4	243 ± 5	242 ± 5

[a] The data points of the signal recovery were fitted according to $I_0 - I_1 \cdot \exp(-t/T_1)$.

Thus there are two contributions to the relaxation rate T_1^{-1} that are weighted by factors which are given by the populations p_1 and

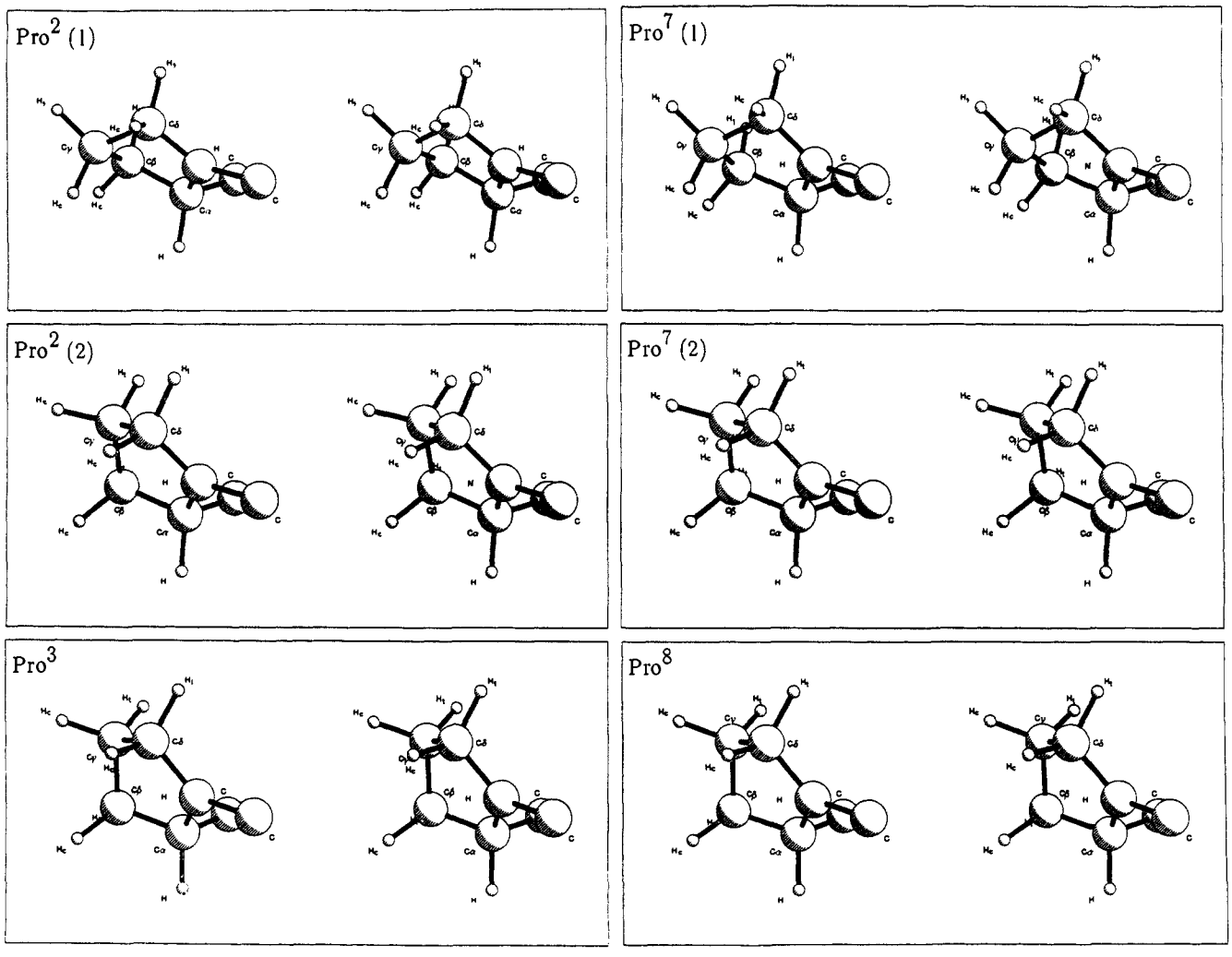

Figure 3. Stereographic representation of the proline ring conformations that conform to the χ angles deduced from the J coupling analysis, listed in Table VII: the two conformations of Pro^2, the conformation of Pro^3, the two conformations of Pro^7, and the conformation of Pro^8.

p_2 (with $p_1 + p_2 = 1$) of the two proline conformations and by the jump angle $\Delta\theta$ of the vector $\mathbf{r}_{CH}$ under the conformational transition. The first contribution depends exclusively on the correlation time τ_c of the molecular tumbling process, whereas the second contribution depends on the total correlation time $\tau_{tot} = (\tau_c^{-1} + \tau_e^{-1})^{-1}$. N is as usual the number of protons bound to the considered carbon. Other sources of relaxation, such as chemical shielding anisotropy or scalar relaxation through coupling to ^{14}N, are negligible. The influence of a vicinal proton on ^{13}C relaxation, for example, is by a factor 60 smaller than the effect of a directly bounded proton.

In order to evaluate eq 4, the jump angle $\Delta\theta$ must be known for the ^{13}C–H internuclear vectors under the ring flip process. To separate the overall tumbling motion of the molecule, that is irrelevant for the ring-flip-induced relaxation, it is necessary to determine the jump angles $\Delta\theta$ in a molecule-fixed coordinate system that refers to the (almost) rigid backbone. It appears best to attach the molecular coordinate system to the principal axes of the molecular tensor of inertia. Here, we have used two approximate approaches: (i) The nuclei N^{Pro} and C_α^{Pro} as well as the center of the interconnecting line of the two adjacent carbonyl carbons C_i' and C_{i-1}' define the rigid molecular plane. (ii) The two carbonyl carbons C_i' and C_{i-1}' as well as the center of the C_α–N bond define the rigid molecular plane. The coordinates of the proline ring have been adjusted to satisfy the dihedral constraints derived from the measured J coupling constants. The resulting jump angles $\Delta\theta$ are indistinguishable for the approaches (i) and (ii) and are given in Table IX.

The correlation time τ_c for the isotropic overall molecular rotation can be obtained from the ^{13}C T_1 relaxation time of the backbone carbons that are not affected by the proline ring flips.

Table IX. Bond Flip Angles $\Delta\theta$ Angles (in deg) for the Pro^2 and Pro^7 Conformations Determined by Either One of the Two Approaches (i) and (ii) as Discussed in the Text

$\Delta\theta$	C_α–H	C_β–H	C_γ–H	C_δ–H
Pro^2	4	50	75	35
Pro^7	1	44	76	41

On the basis of the T_1 values of the α carbons listed in Table VIII, one finds $\tau_c \simeq 300$ ps, a value that lies in the expected range for a molecule of this size dissolved in chloroform.

The correlation time τ_e of the proline ring flips can, in principle, be computed based on the measured ^{13}C T_1 values of Table VIII together with the $\Delta\theta$ values in Table IX, obtained from the J coupling constants, by evaluating eq 4. In order to visualize the (limited) accuracy with which τ_e can be derived in this way, an inverse procedure shall be used: For an assumed correlation time τ_e, the range of $\Delta\theta$ values compatible with measured T_1 value are calculated, taking into account a ±5% error for T_1 which is more than the error listed in Table VIII from two independent T_1 measurements. This leads for the β, γ and δ carbons of Pro^2 and Pro^7 to the feasible $\Delta\theta$ ranges plotted in Figure 4 as functions of τ_e. At the same time, the $\Delta\theta$ values of Table IX taking into account an estimated error of ±6.5° are visualized by horizontal bars in Figure 4. This error estimate is justified by the rms deviation of ±5° of dihedral angles determined from the modified Karplus equations.[28-30] The black cross sections of the two areas in Figure 4 indicate the range of τ_e values compatible with the experiments. The most likely τ_e value is chosen to be the value at which the sum of the black cross sections for each proline residue is maximum. This leads to the values $\tau_e \simeq 30$ ps for Pro^2 and

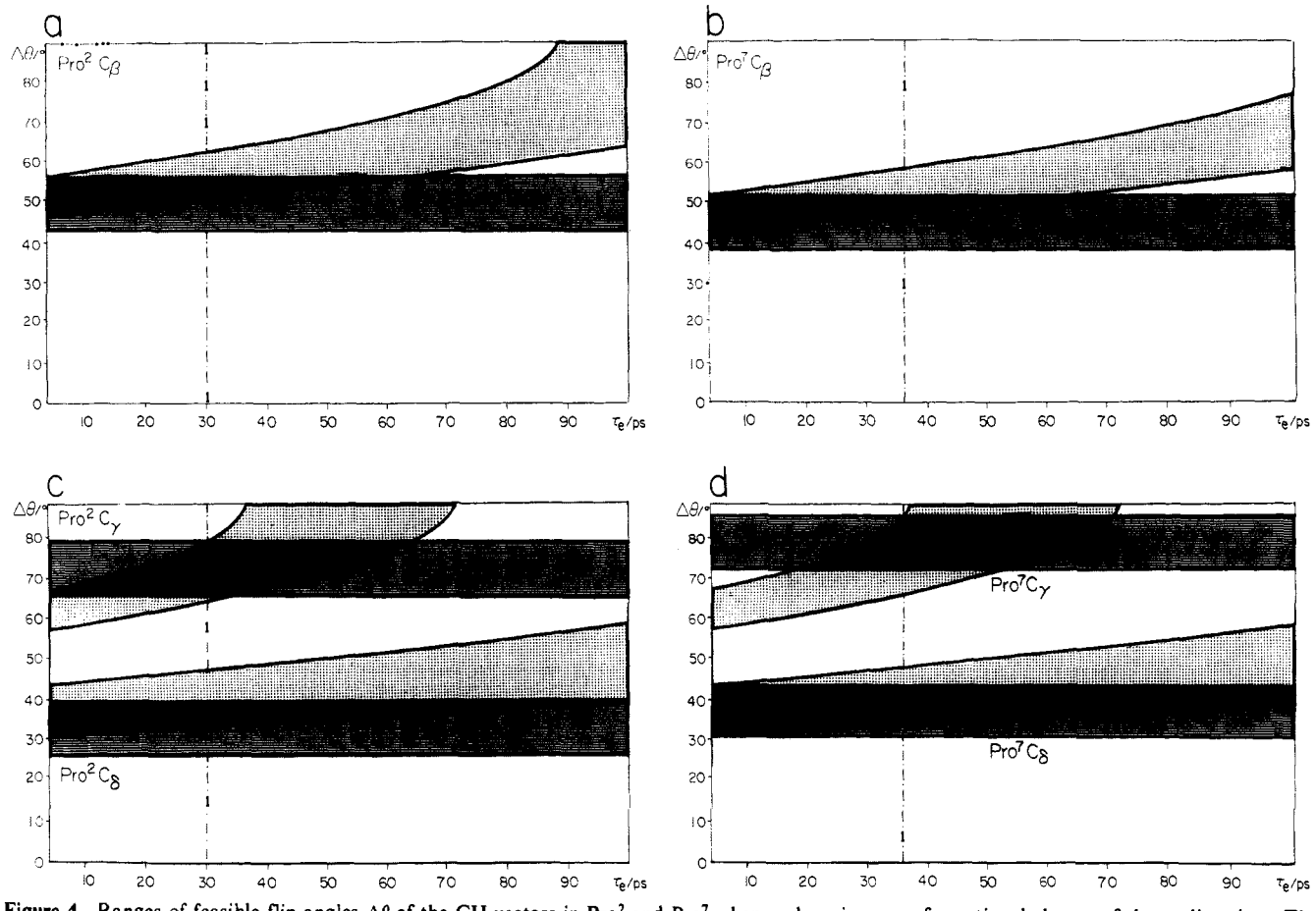

Figure 4. Ranges of feasible flip angles $\Delta\theta$ of the CH vectors in Pro^2 and Pro^7 when undergoing a conformational change of the proline ring. The angles $\Delta\theta$ in the curved or inclined areas are determined as functions of the correlation time τ_e in such a way as to satisfy via eq 3 the measured T_1 relaxation times. At the same time, the ranges of feasible $\Delta\theta$ values computed from the measured vicinal J coupling constants are indicated by horizontal areas with a width of 13°. The overlap areas that indicate agreement between J coupling constants and relaxation measurements are shown in black. The correlation times τ_e at which the total overlap for β, γ, and δ carbons is maximal are marked by a broken line.

$\tau_e \simeq 36$ ps for Pro^7 with a large uncertainty that can be appreciated from Figure 4.

6. Discussion

It is interesting to compare the flexibility of proline residues in antamanide with predictions derived by Cung et al.[22] from crystal structures of proline-containing peptides. They concluded that conformational dynamics of prolines is possible only for an angle $\chi_0 \simeq \varphi + 60°$ within the limits $-15° \leq \chi_0 \leq 10°$. Within these limits two conformations with nearly equal population can coexist, whereas outside of this range only one conformation is feasible. This is a result of strain imposed by the peptide backbone onto the proline residue. The χ_0 values in Table VII reveal that indeed Pro^2 and Pro^7 are expected to exist in two conformations as χ_0 is well within the indicated range. On the other hand, the χ_0 values for Pro^3 and Pro^8 are both at or outside the lower limit of the range that allows dynamics.

Evidently the antamanide backbone conformation determines whether proline ring dynamics is possible. However, the present study shows that the proline ring flip motion, when occurring, is a process that is not correlated with the conformational dynamics of the backbone. The rate constant of 3×10^6 s^{-1} for the backbone conformational motion, measured by Burgermeister et al.,[12,13] is by a factor of 10^4 slower than the proline ring flips observed in the present work. This obviously precludes any correlation. The independence of the two motions is also reflected in the small change of the backbone angle $\chi_0 \simeq \varphi + 60°$ induced by the ring flip. The correlation time of ~30 ps for the proline ring flips is in qualitative agreement with the values estimated by London for other peptides in solution.[18] It is also in agreement with values observed in the solid state by Sarkar et al.[20,21]

The detailed analysis of the cross peak multiplet structure in two-dimensional spectra has proved to be a fruitful approach for obtaining valuable J coupling information that can be exploited for the determination of molecular structure of amino acid residues in peptides. Moreover the coupling constants can be used to quantitatively elucidate conformational equilibria. In combination with relaxation time measurements, it is also possible to determine the motional correlation times of the conformational processes.

The J coupling information obtained could not have been easily extracted from one-dimensional spectra because of severe overlap of the various proline subspectra for antamanide. Even in the 2D E.COSY spectrum, that exhibits maximum simplicity in the multiplet patterns, overlap of cross peaks occurs. The application of iterative computer fitting procedures has turned out to be indispensible. These procedures are quite time-consuming but allow a full analysis even in the case of strong coupling that prevents a straightforward step-by-step analysis.

Obviously for very large proteins where the line width dominates the multiplet splittings, the procedure becomes more difficult to be applied, and the error limits increase. However as long as cross peaks in COSY-like spectra are visible, it will always be possible to determine at least the dominant J coupling constants by such an iterative computer procedure. Even a limited set of coupling constants may prove to be valuable for the analysis of molecular structure and dynamics.

Acknowledgment. This research has been supported by the Swiss National Science Foundation (Project No. 2.075-0.86) and by the Kommission zur Förderung der wissenschaftlichen Forschung (Project No. 1540). We thank Dr. A. Müller and Prof. Dr. H. Kessler, Frankfurt, for the antamanide sample and for sending refs 9 and 10 prior to publication. The manuscript has been processed by I. Müller.

Registry No. Antamanide, 16898-32-1; proline, 147-85-3.